DESIGN AND EXPERIMENT OF A CORN INTER-PLANT WEEDING MACHINE BASED ON VISUAL RECOGNITION

/

基于作物株距信息识别的杂草精准清除机设计与试验

JingWen ZHANG [1,2], QiangJi PENG[3,4], JianMing KANG[3,4], ZhiFeng DI[3,4], ShaoWei WANG[3,4], YingKai CHEN[3,4], YuLong CHEN[1,2*]

[1] School of Agricultural Engineering and Food Science, Shandong University of Technology, Zibo, China

[2] Institute of Modern Agricultural Equipment, Shandong University of Technology, Zibo/China

[3] Shandong Academy of Agriculture Machinery Sciences, Jinan, China

[4] Huang Huai Hai Laboratory of Modern Agricultural Equipment, Ministry of Agriculture and Rural Affairs, Jinan/China

E-mail: cyl06471@sdut.edu.cn

Corresponding author: Yulong Chen

DOI: https://doi.org/10.35633/inmateh-75-73

***Keywords:** agricultural machinery, skeletonization, image stitching, corn interplant recognition*

ABSTRACT

To address the challenges associated with high interrow weeding difficulty and seedling damage in corn fields, a weed removal machine based on crop spacing recognition was designed. It captures crop images at variable speed intervals, obtains corn seedling centroid coordinates via image stitching and skeleton extraction, calculates actual plant spacing through pixel-to-real coordinate transformation, and enables real-time control of the weeding device. Key components were analyzed for motion trajectories and critical parameters. Field tests revealed optimal performance at 0.45 m/s, namely, a 92.6% weed removal rate with 2.05% seedling damage, meeting operational requirements. This research provides technical and equipment support for interrow weeding.

摘要

针对大田玉米株间除草难度大、伤苗率高的问题，设计了一种基于作物株距信息识别的杂草清除机。依据车速信息变化间隔拍摄作物图像，通过图像拼接与骨架提取获取玉米苗质心坐标，结合像素坐标系与实际坐标系之间的转换原理计算出两作物实际株距，控制系统根据株距信息实时控制除草装置；对关键部件除草装置进行设计分析，分析除草运动轨迹，明确影响运动轨迹的关键参数。在设计分析的基础上进行田间试验，试验结果表明，当前进速度为0.45m/s 时，除草效果较好，除草率为92.6%，伤苗率为2.05%，满足作业要求，该研究可为株间除草提供技术和装备支撑。

INTRODUCTION

Weeds compete with crops for nutrients and space for growth, severely affecting crop yield and quality *(Uehleke et al., 2024; Zheng et al., 2024)*. Efficient weed control is a key link in agricultural production. At present, field weeding is performed via three main methods: manual weeding, chemical weeding, and mechanical weeding *(Wang et al., 2021)*. Manual weeding is characterized by a high labor intensity, low efficiency, and high operating costs *(Fang et al., 2022)*; chemical weed control poses problems such as environmental pollution and harm to the health of workers *(Ji et al., 2023)*; and mechanical weeding has the advantages of reduced labor and high efficiency and is an inevitable choice for the development of modern agriculture *(Lai et al., 2023)*. Improving the accuracy of crop center distance recognition in field operation environments is a key prerequisite for achieving interplant weed control operations.

Domestic and foreign scholars have conducted extensive research on interplant mechanical weed control for field crops. *Pérez Ruiz et al. (2014)* designed an interplant weed control device with a cylinder-driven opening and closing for hoes, which requires human–machine collaboration. *Jiao et al. (2023)* developed a device for weed control between rows in paddy fields and conducted field experiments.

Quan et al. (2021) designed a weed control mode based on corn root protection to address the problem of crop root damage in weed control with mechanical actuators. They also designed an intelligent plant weed control robot system to detect corn seedlings and weeds through YOLOv4 and conducted field experiments. The above research yielded several useful conclusions, but owing to issues such as work speed and performance limitations, there are currently no mature products available on the market *(Xing et al., 2022)*.

A crop center recognition method is proposed to address the problems of high computational complexity and low efficiency in intelligent weed control algorithms. The proposed method uses machine vision to obtain the crop centroid and coordinate system transformation to obtain the actual distance between two crops. Image stitching technology is used to continuously obtain crop plant distance information, and the control system controls the rotation speed of the weed control device in real time on the basis of the plant distance information, thereby achieving interplant weed control in corn fields.

MATERIALS AND METHODS

Structure and working principle of the weed removal machine

The overall structure of the machine, which is shown in Figure 1, includes a self-propelled chassis, industrial cameras, weed control devices, etc. The overall structure is based on the self-propelled chassis, and the weed control device is installed at the lower middle position of the chassis.

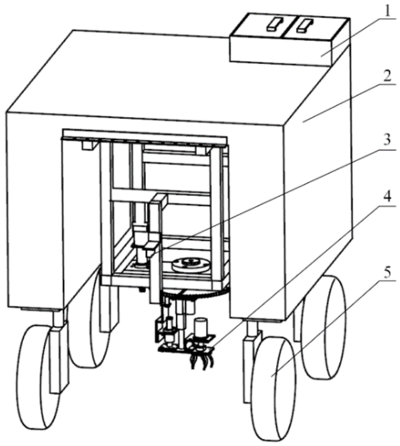

Fig. 1 - Structural diagram of the weed control device test prototype

1. Control system; 2. Self-propelled chassis; 3. Industrial camera; 4. Weed removal device; 5. Wheel hub motor

Table 1

Main technical parameters of the weed removal device

Parameters	Value
Size of whole machine (length×width×length)/(mm×mm×mm)	1,000×800×400
Power/kW	25.2
Work speed/(m/s)	0.45
Control width/mm	240
Speed range of the weed removal device/(r/min)	30-40

Identification and localization methods for corn sprouts

The overall structure of algorithm used in the weed removal and machine plant spacing recognition system is shown in Figure 2. Plant images are taken at intervals on the basis of vehicle speed information, and a feature point matching mechanism and the fusion of different frequency bands are used to preserve details for image stitching. According to traditional machine vision methods, the image is processed, and the plant centroid is obtained by refining the skeleton and comparing the skeleton intersection points with the contour centroid. Finally, the plant spacing information is obtained by converting between the global coordinate system and the pixel coordinate system.

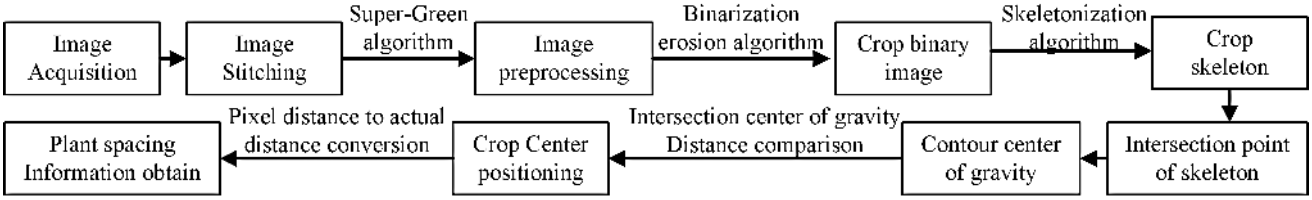

Fig. 2 - Overall algorithm structure

Original image acquisition

By continuously capturing images of seedlings through a vehicle-mounted industrial camera and adjusting the shooting time according to changes in vehicle speed, plant images are obtained, as shown in Figure 3.

Fig. 3 - Example seedling images captured with the device's camera

Image mosaicking

The scale-invariant feature transform (SIFT) algorithm is used to detect key points in the images and generate scale-invariant and rotation-invariant descriptors. A BFMatcher object is created, the KNN-Match method is utilized to match the feature descriptors between two images, the parameter K=2 is set, and the Euclidean distance for each feature point is returned.

$$d = \|v_1, v_2\| = \sqrt{\sum_{i=1}^{128} (v_{1i} - v_{2i})^2} \tag{1}$$

Here, v_1 and v_2 are 128-dimensional SIFT descriptor vectors.

A ratio test is applied to filter reliable matching points if the first-best match distance d_1 and the second-best match distance d_2 of a feature point satisfy:

$$\frac{d_1}{d_2} < 0.75 \tag{2}$$

In this case, the match is considered valid. Figure 4 shows the process of stitching two images together.

Fig. 4 - Stitching of two images

a. Feature points; b. Feature point matching

The homography matrix H is computed by matching point pairs, and the second image is projected to the coordinate system of the first image.

The homography transformation is defined as follows:

$$\begin{bmatrix} x' \\ y' \\ 1 \end{bmatrix} = H \begin{bmatrix} x \\ y \\ 1 \end{bmatrix} = \begin{bmatrix} h_{11} & h_{12} & h_{13} \\ h_{21} & h_{22} & h_{23} \\ h_{31} & h_{32} & h_{33} \end{bmatrix} \begin{bmatrix} x \\ y \\ 1 \end{bmatrix} \tag{3}$$

The optimal homography matrix H is iteratively estimated via the RANSAC algorithm by minimizing the reprojection error, defined as:

$$\arg\min_{H} \sum_{i} \left\| x_i' - Hx_i \right\|^2 \tag{4}$$

After alignment is complete, the second image undergoes perspective rotation to match the angular orientation of the first image. The final image stitching result is shown in Figure 5.

Fig. 5 – Result of image stitching

Image preprocessing

Figure 6 shows the image preprocessing process for a single crop. The collected images are preprocessed via an ultragreen algorithm and area threshold segmentation. The corrosion algorithm is used for weed and plant seedling recognition, weed images are removed, and agricultural plant seedling images are extracted.

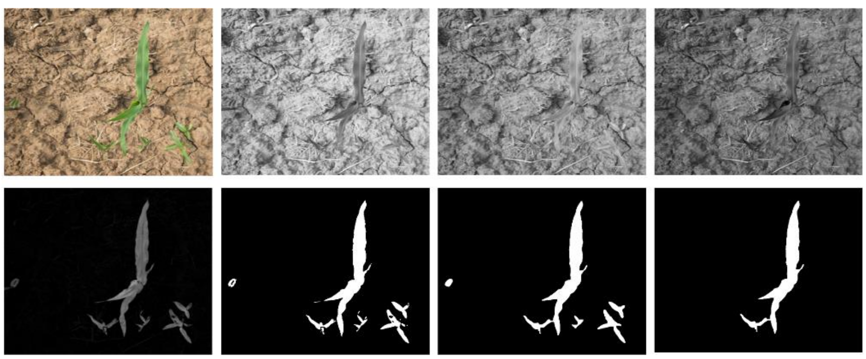

Fig. 6 - Image preprocessing

a. Original image; b. blue channel; c. green channel; d. red channel; e. excess green (ExG); f. binarization; g. morphological opening/closing; h. area threshold segmentation

Skeletonization

The principle of skeleton refinement is shown in Figure 7. First, the image is converted into a binary image by setting a threshold to retain only the contour regions of crop seedlings. The contour information is extracted via the findContours function in the OpenCV library, and the bounding box of each contour is calculated with its center coordinates expressed as:

$$c_x, c_y = \left(\frac{x_{\min} + x_{\max}}{2}, \frac{y_{\min} + y_{\max}}{2} \right) \tag{5}$$

where (x_{min}, x_{max}, y_{min}, y_{max}) are the extreme coordinates of the contour's bounding box

Starting from the center, the radius is iteratively expanded in increments of ΔR to verify the tangency condition between the circle and the contour.

$$\sum_{(x,y)\in\partial M} \delta\left(\sqrt{x - c_x^{\ 2} + y - c_y^{\ 2}} - R_k \geq 2 \right) \tag{6}$$

In the equation, δ represents the Dirac delta function, which is applied to determine the number of points on the contour where the distance equals the current radius R_k. At least two points must satisfy the tangency condition for this criterion to hold.

The process is further refined via the Zhang–Suen thinning algorithm *(Wu et al., 2022)* to iteratively erode edge pixels layer by layer, preserving a single-pixel skeleton. The pixel deletion conditions of the algorithm are as follows:

$$\begin{cases} N\left(p\right)=\sum_{i=1}^{8} p_i (Total\ number\ of\ pixels\ in\ the\ domain) \\ B\left(p\right)=\sum_{i=8}^{8} \left|p_i - p_{i+1}\right| (Numberofboundarytransitions) \end{cases} \tag{7}$$

If the following conditions are met,

$$2 \leq N(p) \leq 6\ and\ B(p) = 2 \tag{8}$$

the pixel p is deleted to preserve the centerline. All circles within the contour are detected, and their center coordinates are connected to ensure that the skeleton maintains a single-pixel width. The trajectory formed by linking these circle centers constitutes the crop contour skeleton.

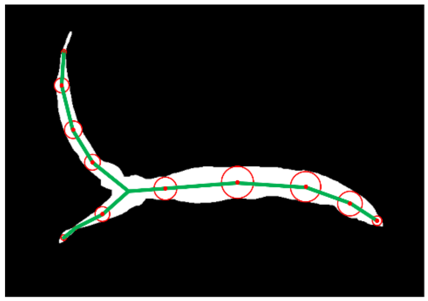

Fig. 7 - Skeleton thinning

Crop contour centroid acquisition

The matching process combines skeleton junction points and contour centroids. For each pixel $p(x,y)$ in the skeleton image, its 8 neighborhood pixels are examined, and the neighborhood coordinates are defined as:

$$\begin{cases} d_x = -1,0,1,1,1,0,-1,-1 \\ d_y = 1,1,1,0,-1,-1,,-1,0 \end{cases} \tag{9}$$

with 8-neighborhood traversal in a clockwise order.

A pixel p is identified as a junction point if its neighborhood contains at least three skeleton pixels. The mathematical condition is defined as follows:

$$\sum_{i=1}^{8} S\left(x+d_{xi}, y+d_{yi}\right) \geq 3 \tag{10}$$

In the equation, $S(x,y)$ represents the pixel value of the skeleton image at coordinates (x,y), where 1 denotes the skeleton and 0 corresponds to the background.

The centroid coordinates (c_x, c_y) of the contour are calculated via image moments via the following formula:

$$c_x = \frac{M_{10}}{M_{00}}; c_y = \frac{M_{01}}{M_{00}} \tag{11}$$

where the image moment M_{pq} is defined as:

$$M_{pq} = \sum_x \sum_y x^p y^q I\left(x,y\right) \tag{12}$$

In the equation, $I(x,y)$ represents the binary image, M_{00} corresponds to the contour area, and M_{10} and M_{01} are the first-order moments.

The skeleton junction point closest to the contour centroid is selected as the stem centroid. The Euclidean distance is calculated as follows:

$$d^* = \min_{\left(x,y\right) \in set\ of\ Intersection\ Points} \sqrt{\left(x_i - c_x\right)^2 + \left(y_i - c_y\right)^2} \tag{13}$$

The final localization result is illustrated in Figure 8.

Fig. 8 - Identification results for individual seedlings

a. Skeleton refinement results; b. junction points of the skeleton; c. contour centroid; d. plant centroid positioning results

Acquisition of plant spacing information

The camera is calibrated to obtain the intrinsic parameter matrix, which includes the focal length (f_x, f_y) and the principal point (C_x, C_y). The camera intrinsic parameter matrix is expressed as:

$$Z=\begin{bmatrix} f_x & 0 & C_x \\ 0 & f_y & C_y \\ 0 & 0 & 1 \end{bmatrix} \tag{14}$$

The centroid pixel coordinates of two corn plants are converted into coordinates in the image coordinate system. This conversion is based on the camera's intrinsic matrix and requires subtracting the principal point coordinates from the x and y values of the pixel coordinates and then dividing by the focal length to obtain the u and v values in the image coordinate system.

$$\begin{cases} u=\dfrac{x-C_Z}{f_z} \\ v=\dfrac{y-C_y}{f_y} \end{cases} \tag{15}$$

where (x, y) represents the centroid's pixel coordinates and (u, v) represents the coordinates in the image coordinate system.

Furthermore, given that the depth information for the camera in the corn field is d, with d, the points in the image coordinate system are converted into points in the camera coordinate system, and the actual distance between the two corn plants in three-dimensional space is calculated. The coordinate calculation formula in the camera coordinate system is as follows:

$$\begin{cases} X=u\cdot d \\ Y=v\cdot d \\ Z=d \end{cases} \tag{16}$$

where d represents depth information, which is the distance from the camera to the corn plants in the vertical direction.

The actual distance between two corn plants is calculated via the distance formula between two points in three-dimensional space:

$$D_L=\sqrt{\;X_2-X_1\;^{2}+\;Y_2-Y_1\;^{2}+\;Z_2-Z_1\;^{2}} \tag{17}$$

where (X_1, Y_1, Z_1) and (X_2, Y_2, Z_2) are the global coordinate sets of two adjacent seedlings.

The final positioning result is shown in Figure 9.

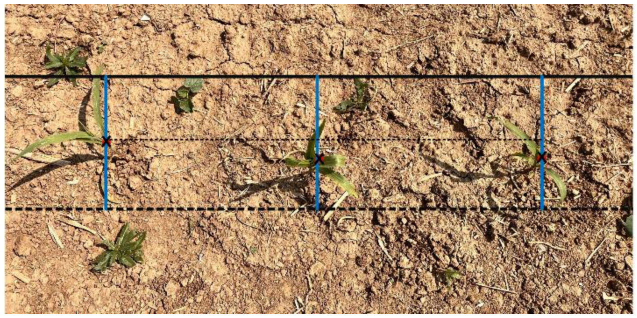

Fig. 9 - Results of interplant seedling identification and localization

Design and analysis of weeding devices

Weeding device design

The weeding device consisted of a support frame, a power transmission device, and a gear set, as shown in Figure 10. The weeding device is attached to the support frame, with the power transmission device acting as the core power provider for the weeding device. Power is transmitted to the small gear via coupling, and the small gear drives the large gear to rotate. The control system, which is based on the plant spacing information from the recognition system and the forward speed, controls the rotation speed of the weeding device in real time. Under the combined action of the rotation of the weeding device and the movement of the self-propelled chassis, the weeding tines form a cycloid trajectory on the ground *(Huang et al., 1979)*, ensuring that the center of the crop canopy is located at the center of a single cycloid trajectory, thus weeding without damaging the seedlings.

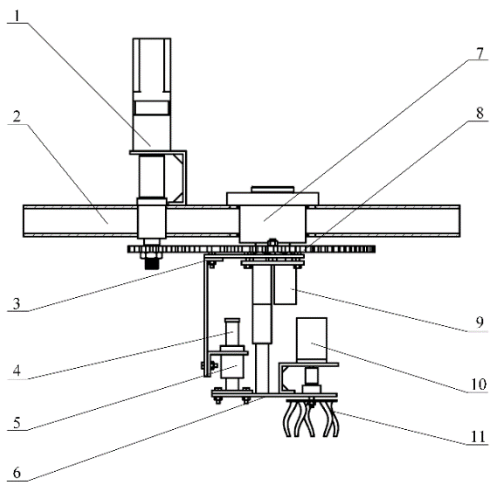

Fig. 10 - Schematic diagram of the rotating device structure

1. Power take-off; 2. Bracket support; 3. Support plate; 4. Optic axis; 5. Linear bearing; 6. Traditional support plate for weed removal; 7. Bearing housing; 8. Gear set; 9. Linear actuator; 10. Weed removal DC motor; 11. Weeding teeth

Weed removal trajectory analysis

The maximum major axis value L (defined as the distance between points A and B) and the maximum minor axis value S (defined as the distance between points C and D) were set to approximately 1. This configuration enabled effective prevention and removal of interrow weeds, and the trajectory variation of the cutting tool was the primary focus of the optimization analysis.

Optimization of parameter L

As shown in Figure 11, assuming that the intersection point of circle O and the y-axis is F, a perpendicular extension line passing through point F intersects the cycloid at point E, and a perpendicular extension line passing through point E intersects the x-axis at point E'. If the time taken for point E to complete a rotation is t, according to the theory of cycloids, the time required for point B to rotate is the same as that of point B', and the time required for point B' to rotate is $t/2$.

Thus, it can be obtained:

$$t=\frac{2\pi R}{\lambda u_x}\Rightarrow\frac{t}{2}=\frac{\pi R}{\lambda u_x} \tag{18}$$

where t - rotation time of point F around the circle, [s];
R - the radius of circle O, [mm];
λ - the ratio of forward speed u to rotational speed v;
u_x—velocity of circle O in the x-axis direction, [m/s];

The abscissa value of point B is the same as that of point A'; therefore,

$$l_{OA'}=u_x\frac{t}{2}=u_x\frac{\pi R}{\lambda u_x}=u_x\frac{\pi R}{\lambda} \tag{19}$$

The intersection circle O of BO and AO is connected to two points D and C. Let the arc length CK be l_1 and the arc length KD be l_2. From the arc length formula, it can be obtained:

$$l_1=\theta_1 R\Rightarrow\theta_1=\angle COK=\frac{l_1}{R},\left(0<\theta_1<\frac{\pi}{2}\right),\quad l_2=\theta_2 R\Rightarrow\theta_2=\angle KOD=\frac{l_2}{R},\left(0<\theta_2<\frac{\pi}{2}\right) \tag{20}$$

According to the Pythagorean theorem:

$$AA'=l_{OA'}\cdot\tan\theta_1=l_{OA'}\cdot\tan\left(\frac{l_1}{R}\right);A'B=l_{OA'}\cdot\tan\theta_2=l_{OA'}\cdot\tan\left(\frac{l_2}{R}\right) \tag{21}$$

Then,

$$AB=l_{OA'}\left(\tan\theta_1+\tan\theta_2\right)=l_{OA'}\left(\tan\left(\frac{l_1}{R}\right)+\tan\left(\frac{l_2}{R}\right)\right) \tag{22}$$

where

$$l_{OB}=\sqrt{\left(l_{OA}\right)^2+\left(l_{OA'}\tan\theta_2\right)^2}=\sqrt{\left(l_{OA}\right)^2\left(1+\tan^2\theta_2\right)};\quad l_{OA}=\sqrt{\left(l_{OA}\right)^2+\left(l_{OA'}\tan\theta_1\right)^2}=\sqrt{\left(l_{OA}\right)^2\left(1+\tan^2\theta_1\right)} \tag{23}$$

Let $\theta_1+\theta_2=\theta_J$, $(0<\theta_J<\pi)$, and $AB=L$. According to the sine theorem:

$$L=\frac{l_{OB}}{\sin\left(90^{\circ}+\theta_2-\theta_J\right)} \tag{24}$$

Notably, L is an increasing function with respect to θ_J within $(0, \pi/2)$ and a decreasing function with respect to θ_J within $(\pi/2, 0)$.

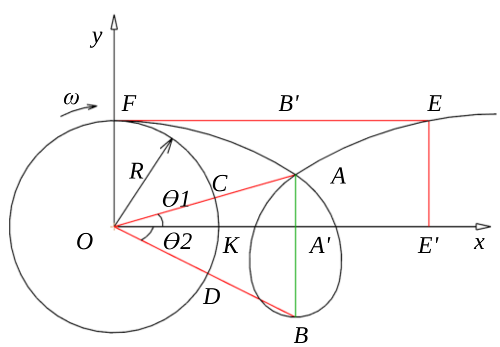

Fig. 11 - Optimization of parameter L

Optimization of parameter S

As shown in Figure 12, from $\omega t=\theta$ and $x=vt+Rsin\,\omega t$, it can be obtained:

$$x=\frac{v}{\omega}\theta+Rsin\theta x \tag{25}$$

With respect to x, the derivative of θ is obtained:

$$\frac{d_x}{d_\theta} = \frac{v}{\omega} + R\cos\theta,\ \theta_J < \theta < \pi \tag{26}$$

When $dx/d_\theta=0$, the extremum is:

$$\cos\theta_{\max} = -\frac{v}{\omega}\frac{1}{R} \tag{27}$$

$$\theta_{\max} = \arccos\left(-\frac{v}{\omega}\frac{1}{R}\right), \theta_J < \theta_{\max} < \pi \tag{28}$$

The maximum transverse chord value is as follows:

$$S = 2\left(\frac{v}{\omega}\theta_{\max} + R\sin\theta_{\max} - l\right) \tag{29}$$

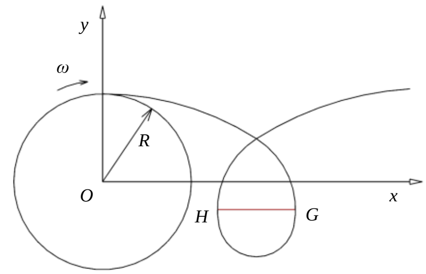

Fig. 12 - Optimization of parameter S

According to formulas (24) and (29), the values of parameters L and S are related to the turning radius, turning speed, and forward speed of the equipment. After image recognition analysis yields the plant spacing value, the turning speed and turning radius are adjusted in a timely manner in combination with the forward speed.

Design principles of the weed control machine control system

The controller detects the distance information between the weeding tines and the ground through a distance sensor and drives the weeding motor to ensure the high-speed rotation of the tines. A speed encoder and the NVIDIA Jetson TX2 microprocessor work in a loop to monitor the chassis travel speed and the crop center distance for the controller. After the relative position information of the seedlings is obtained, the controller adjusts the speed of the weeding device by controlling the stepper motor to achieve precise weeding.

Control system hardware and circuit design

The hardware circuit design of the control system is shown in Figure 13. The hardware circuit consists of encoders, STM32F103 microcontrollers, stepper motors, cameras, NVIDIA Jetson TX2 microprocessors, and other components.

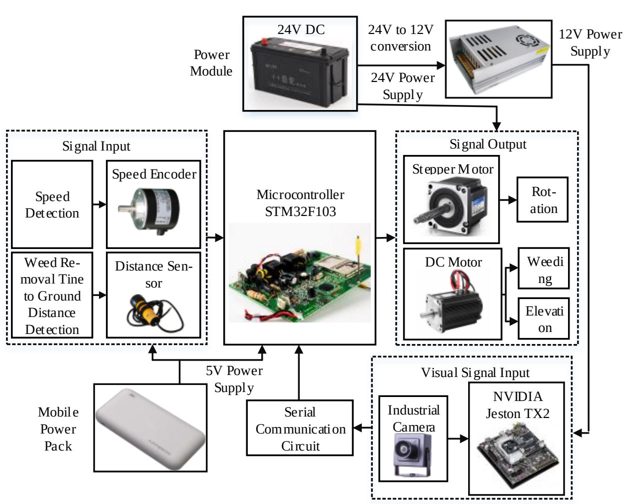

Fig. 13 - Hardware composition of the control system

The working process of the whole machine is as follows: as the chassis advances, the NVIDIA Jeston TX2 microprocessor begins to receive images captured by the camera and recognizes seedlings and weeds. The STM32F103 microcontrollers calculate the center coordinate position of the seedlings and the lateral and longitudinal deviations between the material center and the center of the weeding teeth in the pixel plane. When the seedlings are in the center position of the weeding teeth, the STM32F103 microcontrollers send a start signal to rotate the stepper motor. The microcontroller provides the alpha, beta, and gamma values of the host via a feedback loop on the basis of the recognition image and adjusts the speed of the stepper motor. After the hardware system was assembled, field experiments were conducted to verify the operation of all components of the entire machine.

RESULTS

Experimental conditions

The experiment was conducted on September 8, 2024, at the corn experimental base in Zhangqiu District, Jinan city, using a Nonghaha 2BYQF-3 air suction corn precision seeder with a row spacing of 0.65 meters. For the field performance test, corn seedlings at the 19-day-old and 3-4-leaf stage were selected, with an average stem thickness of approximately 16 mm and a plant height of approximately 25 cm. Five independent experiments were repeated at each forward speed (0.3, 0.4, 0.45, and 0.55 m/s), with a test area length of 16 m. Additionally, the weed control rate and seedling damage rate were recorded for each experiment.

Experimental indicators

In the experiment, weeding efficiency and the seedling damage rate were used as evaluation indicators.

$$P_c = \left(1 - \frac{R_S}{R_H}\right) \times 100\% \; ; \; P_D = \frac{R_D}{R_E} \times 100\% \tag{30}$$

In the formula, P_C represents the weed control rate, %; P_D represents the rate of seedling damage, %; R_S represents weeds that have not been removed after interplant weeding; R_H represents the total number of weeds before weeding; R_D represents the number of injured seedlings; and R_E represents the total number of experimental seedlings.

The experiment was set up with three test areas, each 20 m long. The forward speed of the self-propelled chassis was controlled at a constant speed with a remote controller, with the speed settings ranging from low to high. The starting preparation area was 2 m long, and the test area was 16 m long. The weeds in the test area included naturally occurring *Portulaca oleracea*, *Eleusine indica*, *Capsella bursa-pastoris*, etc. *(Wang et al., 2021),* with the depth of the weed roots being approximately 30 mm. Each test area was marked in advance with prepared signs, and the number of effective corn plants in each area was recorded. The experimental method refers to the "Practical Manual for Field Experiments of Crops," and the field experiment is shown in Figure 14.

Fig. 14 - Experimental scenario

1. Battery; 2. Laptop; 3. Self-propelled chassis; 4. Weeding unit; 5. Hub motor; 6. Weeding tines; 7. DC motor (weeding); 8. Lifting motor (DC); 9. Distance sensor; 10. Gear assembly; 11. Industrial camera; 12. Stepper motor (steering)

Analysis of experimental results

During the bench test analysis of the motion trajectory, a high seedling damage rate was observed. The analysis indicated that the cause was the jerking of the conveyor belt during operation, which led the control system to detect seedlings prematurely, causing a change in the speed of the weeding device and early entry to the weeding area, resulting in seedling damage. In the field test, flat land was chosen, and the self-propelled chassis was moved at a constant speed to avoid the aforementioned situation.

Table 2

Statistics for weeding performance indicators

Test No.	Forward speed/(m/s)	Weeding rate/%	SD (Weeding)	Seedling injury Rate/%	SD (Injury)
1	0.30	91.2 ± 1.5	1.5	2.21 ± 0.18	0.18
2	0.40	91.9 ± 1.2	1.2	2.15 ± 0.15	0.15
3	0.45	92.6 ± 0.9	0.9	2.05 ± 0.10	0.10
4	0.55	90.6 ± 0.9	1.8	2.35 ± 0.25	0.25

The field experiment results (Table 2) revealed that as the advancing speed increased from 0.3 to 0.55 m/s, the weed control rate first increased but then decreased, whereas the seedling damage rate gradually increased. At a speed of 0.45 m/s, the weed removal rate was the highest (92.6%), and the seedling damage rate was the lowest (2.05%). One-way analysis of variance (ANOVA) revealed that different forward speeds had a statistically significant effect on the removal of fast-growing seedlings (F=4.32, p=0.023) and the seedling injury rate (F=3.89, p=0.035) (α=0.05). Multiple comparisons revealed that the weed control rate at a speed of 0.45 m/s was significantly greater than that in the other groups (p<0.05), whereas the seedling injury rate was not significantly different from that in the other groups (p>0.1). The variability analysis of the experimental data revealed that the standard deviation range of the weed control rate was 0.9~1.8%, and the standard deviation range of the seedling damage rate was 0.10~0.25%, indicating high repeatability of the control scheme. The coefficients of variation (CVs) at a speed of 0.45 m/s were 1.6% (weed control rate) and 7.8% (seedling damage rate), indicating stable and reliable machine performance under these operating conditions.

CONCLUSIONS

(1) A corn weeding machine was designed to meet the needs of weeding in corn fields. By using a camera to capture images of plants in the field and applying skeleton extraction algorithms and image stitching techniques to obtain real-time distances between plants, the control system accurately controls the speed of the weed control device on the basis of the distance information between plants.

(2) The key components of the weed control device were designed, and the motion trajectory of the cycloid of the weed control device was analyzed. The turning radius, turning speed, and forward speed were determined to be the key parameters affecting weed control.

(3) In field experiments, the chassis moved at a constant speed, and the results revealed that at a travel speed of 0.45 m/s, the weed control effect was good, with a weed control rate of 92.6% and a seedling damage rate of 2.05%, meeting the agronomic requirements for weed control in corn fields.

Future directions and applications:

To further enhance the practicality and impact of the proposed technology, future research could focus on the following tasks:

Algorithm Optimization: Deep learning models (e.g., convolutional neural networks) could be integrated into the proposed approach to improve real-time weed recognition accuracy under complex field conditions, including overlapping foliage and variable lighting.

Multi-crop adaptability: The system could be extended to other row crops (e.g., soybeans and cotton) by adjusting the plant spacing recognition algorithm and mechanical structure to accommodate diverse growth patterns.

These advancements could accelerate the adoption of intelligent weeding systems in sustainable agriculture, thus supporting the transition toward fully automated and eco-friendly farming practices while addressing global challenges related to food security and environmental conservation.

ACKNOWLEDGEMENT

This study was funded by the Shandong Science and Technology Innovation Project (CXGC2024A09) and the Provincial Science and Technology Innovation Development Project (2022SZX46). We would like to thank all the reviewers who participated in the review. We also want to thank the funders of this project. We sincerely thank you for all the support and assistance.

REFERENCES

[1] Fang, H., Niu, M., Xue, X., Ji, C., (2022). Effects of mechanical-chemical synergistic weeding on weed control in maize field (玉米田间机械-化学协同除草的杂草防除效果). *Transactions of the Chinese Society of Agricultural Engineering*, 2022,38(06):44-51. Nanjing/China. DOI: 10.11975/j.issn.1002-6819.2022.06.005

[2] Huang, Q., (1979). An Approximation Method for Finding the Intersection Point of a Cycloid and a Circle (求余摆线与圆的交点的一种逼近方法). *Mathematics in Practice and Theory,* vol. 1979, no. 2, pp. 6-12, Jilin/China.

[3] Ji, J., He, Q., Zhao, L., Li, P., Liu, Y., Wang, X., (2023). Adaptive Fast Integrating Terminal Sliding Mode Tracking Control Technique for Weeding Robot (除草机器人自适应快速积分终端滑模跟踪控制技术). *Transactions of the Chinese Society for Agricultural Machinery*, vol. 54, no. 6, pp. 55-64, Sichuan/China. DOI: 10.6041/j.issn.1000-1298.2023.06.006

[4] Jiao, J., Hu, L., Chen, G., Tu, T., Wang, Z., Zhang, Y., (2023). Design and experiment of an inter-row weeding equipment applied inpaddy field (水田行间除草装置设计与试验). *Transactions of the Chinese Society of Agricultural Engineering*. 2023,39(24):11-22. DOI: 10.11975/j.issn.1002-6819.202306056

[5] Lacroix, C., Pierreux, J., Brostaux, Y., Vandenberghe, C., Dumont, B., (2025). Assessing the combined effects of mechanical and chemical weeding on weed dynamics in winter wheat. *Weed Research*, 2025, 65(1): e12677. Gembloux/Belgium. DOI: 10.1111/WRE.12677

[6] Lai, H., Zhang, Y., Zhang, B., Yin, Y., Liu, Y., Dong, Y., (2023). Design and experiment of the visual navigation system for a maize weeding robot. (玉米除草机器人视觉导航系统设计与试验). *Transactions of the Chinese Society of Agricultural Engineering*. 2023,39(01):18-27. Beijing/China. DOI: 10.11975/j.issn.1002-6819.202210247

[7] Li, Y., Gans, N., (2017) Predictive RANSAC: Effective Model Fitting and Tracking Approach under Heavy Noise and Outliers. *Computer Vision and Image Understanding*, vol. 161, pp. 99-113. Dallas/America. DOI: 10.1016/j.cviu.2017.05.013

[8] Li, Y., Guo, Z., Shuang, F., Zhang, M., Li, X., (2022). Key technologies of machine vision for weeding robots: A review and benchmark. *Computers and Electronics in Agriculture*, 2022, 196: 106880, Guangxi/China. DOI: 10.1016/J.COMPAG.2022.106880

[9] Pérez-Ruiz, M., Slaughter, D. C., Fathallah, F. A., Gliever, C. J., Miller, B. J., (2014). Co-robotic intra-row weed control system. *Biosystems Engineering*, Vol. 126, pp. 45-55. DOI: 10.1016/j.biosystemseng.2014.07.009

[10] Quan, L., Zhang, J., Jiang, W., Li, H., Yang, C., Zhang, X., (2021). Development and Experiment of Intra-row Weeding Robot SystemBased on Protection of Maize Root System. (基于玉米根系保护的株间除草机器人系统设计与试验). *Transactions of the Chinese Society for Agricultural Machine*. 2021,52(12):115-123. Heilongjiang/China. DOI: 10.6041/j.issn.1000-1298.2021.12.012

[11] Uehleke, R., Plettenberg, L. V., Leyer, M., Hüttel, S., (2024). German sugar beet farmers' intention to use autonomous field robots for seeding and weeding. *Journal of Environmental Management*. 2024. PP 122472-122472. Germany. DOI:10. 1016/J. JENVMAN. 2024. 122472

[12] Wang, J., Yan, D., Wang, Q., Tang, H., Wang, J., Zhou, W., (2021). Design and Experiment of Jet-type Paddy Field Weeding Device between Plants (射流式水田株间除草装置设计与试验). *Transactions of the Chinese Society for Agricultural Machinery,* vol. 52, no. 11, pp. 78-85+94, Heilongjiang/China. DOI:10.6041/j. issn.1000-1298.2021.11.008

[13] Wang, J., Weng, W., Ju, J., Chen, X., Wang, J., Wang, H., (2021). Design and Test of Weeder between Rows in Rice Field Based on Remote Control Steering (基于遥控转向的稻田行间除草机设计与试验). *Transactions of the Chinese Society for Agricultural Machinery,* vol. 52, no. 9, pp. 97-105, Heilongjiang/China. DOI: 10.6041 j. issn.1000-1298.2021.09.011

[14] Wang, S., Su, D., Wang, Z., Jiang, Y., Zhang, L., Tan, Y., (2021). Design and Experiments of the Cam Swing Rod Intra-row Weeding Device for Lettuce Farm (凸轮摆杆式生菜株间除草装置设计与试验). *Transactions of the Chinese Society of Agricultural Engineering*, vol. 37, no. 21, pp. 34-44, Beijing/China. DOI: 10.11975/j.issn.1002-6819.2021.21.005

[15] Wu, Y., Wang, J., Wang, Y., (2022). Crop Stem Recognition and Localization Method Based on Skeleton Extraction Algorithm (基于骨架提取算法的作物茎秆识别与定位方法). *Transactions of the Chinese Society for Agricultural Machinery*, vol. 53, no. 11, pp. 334-340, Tianjin/China. DOI: 10.6041/j.issn.1000-1298.2022.11.034

[16] Xing, Q., Ding, S., Xue, X., Cui, L., Le, F., Li, Y., (2022). Research on the development status of intelligent field weeding robot. *Journal of Chinese Agricultural Mechanization*, Vol. 43, No. 8, pp. 173. Nanjing/China. DOI: 10.13733/j.jcam.issn.20955553.2022.08.024

[17] Zheng, H., Li, Z., Shan, Y., Zhu, Y., Xiao, M., (2024). Current and development trends of agricultural machinery weeding technologies and equipment (农田机械除草技术与装备研究现状与发展趋势). *Journal of Nanjing Agricultural University*. 2025,48(02):285-295. Nanjing/China. DOI: 10. 7685/jnau. 202404014